Molecular heterogeneity and differential metabolic signatures in thymic adipocytes

Joon Schwakopf,[1,2,3], Amber R. Syage,[1,3], Anca Franzini,[3,4], Katherine E. Varley,[3,4], Dean Tantin,[1,4]

[1]Department of Pathology, University of Utah School of Medicine, Salt Lake City, UT, USA.
[2]Department of Neurobiology, University of Utah School of Medicine, Salt Lake City, UT, USA.
[3]Huntsman Cancer Institute, University of Utah School of Medicine, Salt Lake City, UT, USA.
[4]Department of Oncological Sciences, University of Utah School of Medicine, Salt Lake City, UT, USA.

Correspondence: dean.tantin@path.utah.edu

Short title: Molecular characterization of thymic adipocytes

Keywords Thymus; T cells; Thymic epithelial cells; adipocytes; aging

Conflicts of interest statement: The authors have declared that no conflict of interest exists

Words in abstract: 180
Words main text: 11,637
Total main display items: 6

SUMMARY

Adipocyte depots throughout the body are physiologically and molecularly distinct. With age, adipocytes increase in and around aged thymi. However, thymic adipocytes completely lack molecular characterization. We developed and optimized methods to isolate adipocyte nuclei from mouse thymi of different ages and sexes. Single-nucleus multiomic analysis of male and female mice aged 4-9 months reveals that thymic adipocytes are heterogeneous, with at least two distinct populations. One subpopulation harbors a transcription and chromatin signature consistent with beige/brown fat. A larger subpopulation more strongly resembles classic white adipose tissue and expresses genes associated with epithelial-to-mesenchymal transition (EMT) and antigen presentation. Analysis of differentially open chromatin in the white compared to beige adipose population identifies binding sites for Foxn1 and HIF-1α/Arnt, consistent with a situation in which thymic white adipose cells emerge from thymic epithelial cells, possibly under hypoxic conditions. Immunofluorescence microscopy confirmed the expression of UCP1 protein in cells within the thymic parenchyma, most prominently in subcapsular cortical regions. These results reveal a complex milieu of thymic adipocytes and identify multiple avenues for directly probing their ontogeny, dynamics and functional significance.

INTRODUCTION

The thymus is the primary site of T cell development and education and thus plays a central role in adaptive immunity and central tolerance [1]. It consists of developing T cells (thymocytes), thymic epithelial cells (TECs), fibroblastic stromal cells and other less abundant cell types. The aging thymus also accumulates abundant and dynamic population of adipocytes [1], which we here term ThyAds.

With age, areas of the thymus devoted to thymopoiesis atrophy and T cell output declines in a process termed thymic involution [2]. Involution is associated with progressive disruption of the cortico-medullary junction, loss of thymic output, and increased adiposity in a manner influenced by biological sex and diet [3]. Attenuation of thymic output contributes to reduced TCR diversity, impaired pathogen response and increased susceptibility to infection [1,4-7]. Additionally, involution can be accelerated by administration of thiazolidinediones, implicating adipocyte expansion in this process [8], however their function in this process is unclear. Thymic involution is conserved across vertebrates and recapitulated in laboratory mice. Although severe infection, radiation, malnutrition, or hormonal alterations can induce acute thymic atrophy, age-related involution is the setting in which adipocyte accumulation is most consistently observed [1,3,9-11]. Despite their increasing abundance in the aging thymus, and the possibility that they have specialized functions analogous to other tissue-specific fat depots [12], ThyAds have yet been directly studied at the molecular level. Prior studies focused on thymocytes and thymic stromal cells have omitted ThyAds because intact adipocytes are large, buoyant, and fragile, and are therefore poorly captured by droplet-based microfluidic workflow [13-16].

Recent single-nuclei methodologies combining RNA-seq and ATAC-seq have enabled high-resolution mapping of adipose depots, including age-associated pro-inflammatory and metabolic shifts linked to obesity and related pathologies. These technologies have also shown that adipose depots are tailored to their local environment and differ in cellular and molecular composition across the body [12], and that adipocytes remodel over time [17,18]. In humans highly metabolically active brown adipose tissue (BAT), subcutaneous white adipose tissue (WAT), and beige fat, an intermediate form, typically decline with age wheras visceral WAT expands [19-21]. Together, these findings led us to hypothesize that ThyAds are distinct from other adipocyte populations and that their age-associated expansion reflects changes in cellular composition and state.

Here, we used an integrated multiomic strategy to generate the first single-nuclei dataset of ThyAds. By profiling nuclei rather than intact cells, multiomic sequencing overcomes the technical limitations imposed by adipocyte size and fragility. We develop methodologies to

efficiently liberate and isolate ThyAds and their nuclei from mouse thymi. By single-nucleus profiling, we identify two highly distinct ThyAd populations, termed ThyAd I and ThyAd II. ThyAd I exhibit a beige fat-like transcriptional program, whereas ThyAd II show features consistent with classic WAT. Notably, ThyAd II-specific accessible chromatin was enriched for consensus sites recognized by Foxn1, the master transcription regulator of TECs. This enrichment suggests a TEC-linked regulatory signature and supports the hypothesis that ThyAd II derive from TECs. Together, our ThyAd multiome resolves two adipocyte programs and provide clues to cellular origin, providing a roadmap to test lineage relationships and functional roles in thymic aging.

RESULTS

ThyAds comprise two discrete subpopulations, one of which has transcriptional hallmarks of beige fat

Thymic adipocytes are technically difficult to recover. We successfully developed an enrichment workflow that combines a retina tissue dissociation protocol and WAT buoyancy-based fractionation, followed by single-nuclei isolation to profile 6-month-old female mice (**Figure 1A**). In mature thymi, scattered multilocular lipid-laden cells are detectable within the subcapsular region, parenchyma, and PVS by ~3 months, while large unilocular white adipocytes become prominent after ~12 months [22]. We therefore reasoned that 6-month-old mice would capture maximal diversity in the ThyAd pool, at a timepoint when thymic output is still preserved but ThyAds are recoverable from a sufficient amount of thymic tissue. After dissection, we extensively cleaned the thymic capsule to minimize contamination while preserving subcapsular and septal ThyAds (**Figure 1B**). Thymi were mechanically and enzymatically digested to generate a single-cell suspension, then fractionated to collect the buoyant adipocyte-enriched layer. Nuclei prepared from the buoyant fraction were robust, with preserved euchromatic and heterochromatic regions and nucleoli (**Figure S1A**).

16 pooled female thymi were used for single-nucleus ATAC-seq plus RNA-seq, yielding 3,610 high-quality nuclei after filtering (**Figure S1B**). Initial uniform manifold approximation and projection (UMAP) clustering indicated substantial hematopoietic carryover, with most nuclei expressing *Ptprc* (*Cd45*) and resolving into expected thymocyte populations based on canonical markers such as *Cd8a*, *Cd4*, *Mki67*, *Hes1* and *Cd5* (**Figure S1C,D**). For example, cluster 8 expressed *Il2ra* but not *Cd8a* or *Cd4*, identifying these cells as DN2/3. Cluster 2 expressed *Cd5* and likely comprised B cells. Cluster 7 expressed *Klrb1c*, which encodes the NK1.1 surface protein. These nuclei are likely derived from iNKT cells. In contrast, signatures of non-hematopoietic thymic stromal populations (TECs, fibroblasts/mesenchyme, endothelium) were minimal or absent. This may reflect either or both a greater abundance of bone marrow-derived cells in the thymus, or a closer apposition of these cells with ThyAds such that they are preferentially carried over with the buoyant fraction following digestion. These data establish a technical framework for ThyAd recovery and set the stage for targeted analysis of the ThyAd compartment.

Two transcriptionally discrete clusters (3 and 10) expressed the canonical adipocyte markers *Pparg* and *Plin1* (**Figure S1C**) as well as *Fabp4* (not shown), consistent with adipocytes. A lipid metabolism gene module further supported adipocyte identity in clusters 3 and 10, whereas cluster 11 (the least abundant cluster) showed weaker and less consistent expression of

119 adipocyte-associated transcripts (**Figure S2A**). We therefore focused on adipocyte clusers 3 and
120 10, yielding 429 high-quality adipocyte nuclei. These nuclei contained a mean of 1533 detected
121 genes and an average depth of 2974 reads per nucleus.

122 We re-clustered adipocyte based on gene expression (RNA-seq UMAP), chromatin
123 accessibility (ATAC-seq UMAP), and a weighted nearest neighbor (WNN) approach that
124 integrates both modalities (**Figure 1C**). This analysis resolved two broad transcriptional programs,
125 termed ThyAd I and ThyAd II, distinguished by differential expression of lipid metabolic genes
126 (**Figure S2B**). A small residual thymocyte cluster expressed *Themis* and *Satb1* (**Figure S3A**) as
127 well as lipid metabolic genes such as *Fasn* (**Figure S2B**) and may reflect doublet nuclei. The
128 remaining clusters lacked thymocyte gene expression and robustly expressed adipocyte markers
129 (e.g., *Pparg*), supporting their adipocyte identity (**Figures S2B** and **S3A**).

130 To define transcriptional states within ThyAds, we identified the top 10 DEGs across
131 clusters. This revealed clear separation between ThyAd transcription programs, with ThyAd I
132 more strongly expressing genes associated with thermogenesis relative to ThyAd II (**Figure S3A**).
133 Restricting analysis to adipocyte nuclei only, we further resolved five distinct ThyAD subclusters–
134 Ia, Ib, IIa, IIb and IIc (**Figure 1D**), consistent with prior evidence showing that ThyAds are
135 morphologically heterogeneous [22].

136 ThyAd Ia nuclei were marked by the expression of Prkar2b and *Fgf14*. In contrast, ThyAd
137 Ib more robustly expressed *Esrrg*, *Ucp1*, and *Cidea* (**Figure 1D**). *Ppara* was also up-regulated in
138 ThyAd Ib (**Table S1**). These genes have been shown to positively regulate beige adipocytes [23-25].
139 These findings strongly suggest that ThyAd I – particularly ThyAd Ib – are beige-like, consistent
140 with work that used imaging to identify UCP1-positive cells detected inside the thymic
141 parenchyma [22]. In contrast, ThyAd II nuclei expressed a distinct program consistent with WAT-
142 like identity (e.g., *Apoe*, **Table S1**) and additional features no observed in ThyAd I. ThyAd IIa was
143 enriched for epithelial-mesenchymal transition (EMT)-associated transcripts including *Prr16* and
144 *Alcam*, while ThyAd IIb/IIc displayed higher levels of *B2m* and *H2-D1* (**Figure 1D**), consistent with
145 increased MHC-I-related gene expression [26]. ThyAd II also expressed *Gpx3*, which has been
146 reported in thymic stromal populations including intermediary fibroblast-like states [27]. Additional
147 feature plots are shown in **Figure S3B**. These results indicate that ThyAd I (in particular ThyAd
148 Ib) resembles beige-like adipocytes, whereas ThyAd II is more WAT-like and exhibits an EMT-
149 /antigen-presentation-associated transcriptional signature.

150 Because ThyAd I and ThyAd II subclusters were readily distinguishable by the
151 thermogenic transcription signature in ThyAd I (**Figure 1D**), we combined the ThyAd Ia+Ib and
152 IIa+IIb+IIc subclusters, and performed differential expression analysis (**Table S2**). Gene

153 expression differences between combined ThyAd I and ThyAd II nuclei are shown in **Figure 2A**.
154 For example, *Prdm16* and *Ppara* were significantly enriched in ThyAd I, encoding transcriptional
155 regulators of beige/brown fat [28,29], while Retn and Prr16 were significantly enriched in ThyAd II,
156 encoding WAT-associated protein Prr16 [30] and the adipokine resistin, a regulator of adipogenesis
157 [31], respectively. Gene ontogeny (GO) analysis further supported functional divergence: ThyAd I
158 was enriched for pathways including "Mitochondrial organization" and "Positive regulation of cold-
159 induced thermogenesis", whereas ThyAd II was enriched for "Epithelial mesenchymal transition"
160 (**Figure 2B**).
161

162 **Single-nucleus ATAC-seq identifies state-specific chromatin accessibility and**
163 **transcriptional factor motif enrichment in ThyAds**

164 In addition to improving resolution of ThyAd states, the ATAC-seq component of the multiomic
165 dataset enables inference of regulatory programs by identifying transcriptional factor (TF) motifs
166 enriched in accessible chromatin. Moreover, because the chromatin state can precede or linger
167 relative to active gene expression, the chromatin states can reflect transcription potential as well
168 as recent enhancer decommissioning, providing information on the possible antecedents for given
169 populations. Because genomic DNA is fully preserved within the nuclei while much of the mRNA
170 is lost, the ATAC-seq portion of the data provides high-quality information on gene expression
171 states in isolated nuclei. We analyzed the ATAC-seq data focusing on genes associated with
172 beige adipocytes: *Ppara*, *Cidea* and *Ucp1*. In all cases, increased chromatin accessibility was
173 highly associated with the ThyAd Ib subcluster (**Figure 3A**). Additional genes are shown as
174 expression and ATAC accessibility feature plots in **Figure S4**.

175 To identify candidate TFs underlying ThyAd state differences, we compared TF motifs
176 enriched in between ThyAd I and ThyAd II. ThyAd I accessible regions were enriched for motifs
177 consistent with adipocyte differentiation and beiging, including EBF, Plagl1, PPAR and Esrrg
178 (**Figure 3B**). In contrast, ThyAd II accessible chromatin was enriched for Foxn1, hypoxia-inducible
179 factor-1 (HIF-1), Wilms tumor protein 1 (WT1), Krüppel-like factor 12 (KLF12), and KLF1 motifs.
180 Notably, Foxn1 is a master transcriptional regulator of thymic epithelial cells [32], suggesting a TEC-
181 linked regulatory imprint in the ThyAd II population. Together with the EMT signature associated
182 with ThyAd II gene expression (**Figure 1D and Figure 2B**), these results are consistent with a
183 model in which ThyAd II white adipose cells arise from TECs. Consistent with this interpretation,
184 transcripts encoding *Ebf2*, *Esrrg* and *Plagl1* were detected in subsets of ThyAD nuclei (**Figure**
185 **S4A**). In contrast, other TFs highlighted by motif enticement (including *Foxn1*) were not detectably
186 expressed, yet displayed accessible regulatory regions (**Figure S4A-B**, **Supplemental Tables**

187 **S1 and S2**), consistent with residual chromatin accessibility following recent TF activity or
188 enhancer decommissioning. Together, the data show increased accessibility at thermogenic loci
189 and enrichment of EBF, PPAR, and ESRRG motifs in ThyAd I, while ThyAd II is enriched for
190 FOXO1, HIF, and KLF1 motifs, consistent with a distinct and possibly TEC-linked regulatory
191 imprint.
192
193 **Younger (4-month-old) male mice harbor ThyAd I and II populations distinct from gonadal**
194 **fat**
195 We also profiled ThyAds from 4-month-old male mice to align sampling with the earlier kinetics of
196 thymic involution in males compared with females [33-35]. Whereas 6-month-old females provided
197 an optional window to capture ThyAd heterogeneity while thymic output remains relatively
198 preserved, we reasoned that males would reach a comparable stage of remodeling at an earlier
199 age. In mice, the thymus reaches near-maximal size around 5 weeks of age and then declines in
200 cellularity. In male C57BL/6 mice, thymic cellularity decreases by approximately 50% by 4 months
201 [36]. This is matched in human thymic tissue 26-49 years old, where the perivascular space (PVS)
202 comprises 50-60% of the thymic compartment and adipose tissue is easily identified [37]. We
203 therefore selected 4 months in males as a practical and biological window to capture ThyAds
204 during an early-to-intermediate phase of involution.
205 We isolated ThyAd nuclei from 6 male mice maintained on standard chow and profiled
206 them by single-nucleus RNAseq. From the same animals, we also collected gonadal (epididymal)
207 white adipose tissue (gWAT) as a visceral fat comparator (**Figure 4A**). As in the female dataset,
208 *Ptprc*+ nuclei carried through purification were manually removed prior to clustering. Joint
209 clustering of ThyAd and gWAT nuclei revealed that the thymic and gonadal adipocyte
210 transcriptomes were largely distinct, with ThyAd nuclei again segregating into two discrete
211 clusters (**Figure 4B**). A rare thymic cluster expressed *Esrrg*, *Ppara* and *Ppargc1b*, consistent with
212 a ThyAd I (beige-like) program (**Figure S5A**). In contrast, the ThyAd II cluster more closely aligned
213 with one of the gWAT clusters, suggesting a more WAT-like transcriptional state (**Figure 4B** and
214 **Figure S5A**). Feature plots confirmed strong expression of *Ppara* and *Esrrg* in ThyAd I (**Figure**
215 **4B-C**). These nuclei were also enriched for *Cidea* and *Ghr* (**Figure S5B**). When clustering thymic
216 nuclei alone, ThyAd I and II remained clearly separable, marked for example by *Ppara* and *Ghr*
217 (growth hormone receptor, **Figure 4D**). The most differentially expressed ThyAd I gene was
218 *Ppara*, whereas ThyAd II was enriched for *Xdh*, *Fabp4*, *Adgrl4*, *Klf12* and *Tgfb2* (**Table S3**).
219 Notably, *Tgfb2* (TGFβ2) has been implicated in promoting thymic [38]. Both populations expressed
220 core adipocyte genes including *Pparg* (**Figure 4D**) and *Cd36* (not shown).

221

222 **UCP1$^+$ cells largely localize within the subcapsular cortical thymic compartment, whereas**
223 **lipid-rich unilocular adipocytes localize to septa and perivascular space**

224 Epicardial/perithymic fat is heterogenous, with some beige-like cells strongly expressing UCP1
225 [39]. Although thymi used for sequencing were obtained from mice younger than 6 months old and
226 were extensively cleaned of extrathymic fat prior to processing (**Figure 1B**), it remained formally
227 possible that the beige-like ThyAd I signal reflected residual contamination outside the capsule.
228 Prior work, however, has identified UCP1$^+$ cells within the thymic parenchyma [22]. To directly
229 access localization, we performed Immunofluorescence on 6-month-old female thymi. For this
230 experiment, thymi were interntionally not cleaned of extrathymic fat, enabling direct comparison
231 of perithymic adipose tissue with intrathymic UCP1$^+$ cells.

232 As expected [39], perithymic fat and connective tissue abutting the thymic capsule was
233 heterogenous, with regions containing large unilocular lipid droplets and others containing
234 densely packed multilocular, BAT-like adipocytes with strong UCP1 staining. In contrast, UCP1$^+$
235 cells within the thymic parenchyma were sparse and exhibited weaker, punctate UCP1. Omission
236 of the primary antibody eliminated both the intra- and extrathymic UCP1 signal (**Figure 5**). In
237 parallel, PPARg staining and BODIPY labeling highlighted adipocytes with large unilocular lipid
238 droplets enriched within thymic septa and the perivascular space, consistent with ThyAd II (**Figure**
239 **S6**). Together, these data support the presence of beige-like ThyAd I cells within the thymic
240 capsule and argue against perithymic contamination as the primary source of the ThyAd I
241 transcriptional program detected by multiomic sequencing.

242 **DISCUSSION**

243 The thymus is a complex organ that facilitates the development and selection of thymocytes,
244 playing an important role in the maintenance of adaptive immunity and central tolerance. Cell
245 types associated with the thymus include thymocytes, TECs, fibroblastic/mesenchymal cells,
246 macrophages, DCs, B cells (particularly in the medulla), mature nonconventional T cells (e.g.,
247 iNKTs), endothelial cells, pericytes and nerves. During normal aging, thymic output declines via
248 a process termed thymic involution, contributing to established characteristics of age-related
249 immune senescence, such as reduced naive T-cell production and TCR diversity, chronic
250 systemic inflammation, and impaired pathogen response [1,37,40]. Involution is associated with
251 disruption of the cortico-medullary junction and increased adiposity [3].

252 Recent advances in single-nuclei methodologies combining RNA-seq and ATAC-seq have
253 been used to investigate the heterogeneity of adipose tissue depots throughout the body [12,41].
254 Separately, they have been used to profile thymocytes and thymic stromal cells [13-16]. However,
255 adipocytes associated with the thymus (ThyAds) remain uncharacterized at a molecular level.
256 Here, we developed methodologies to liberate and isolate adipocyte and their nuclei from mouse
257 thymi. We used an integrated multiomic sequencing strategy to generate the first single-nuclei
258 datasets of ThyAds and identify similarities and differences in transcriptional profiles compared to
259 a peripheral adipose depot. We profiled nuclei from female and male thymi at two different ages,
260 providing the first single-nucleus ThyAd atlas and expanding our understanding of ThyAds and
261 their potential roles in the thymus and during thymic involution. By single-nucleus profiling, we
262 identified two distinct ThyAd populations, termed ThyAd I and ThyAd II.

263 Adipocytes can be identified by their robust uptake and storage of triglycerides as neutral
264 lipid, as well as by release of fatty acids, with the balance regulated by metabolic demand. The
265 cellular and molecular composition of adipose tissue varies throughout the body in a manner
266 adapted to the tissue in which they are embedded [12]. For example, subcutaneous and visceral
267 WAT have distinct developmental origins, mechanisms of expansion and disease associations [42].
268 Adipocytes in different tissues closely interface with immune cells such as macrophages, DCs
269 and iNKTs, again in a manner tailored to the local environment, and can both suppress and
270 exacerbate inflammation depending on context [17,18,43,44]. We hypothesized that ThyAds are
271 qualitatively different from adipocytes in other fat depots, just as adipocytes in these depots are
272 different from one another.

273 snRNAseq revealed that ThyAds express mature adipocyte-associated markers such as
274 *Pparg*, *Fabp4*, and *Plin1*. No thymic preadipocytes were identified based on co-expression of

markers such as *Pdgfra/b*, *Pref1* and *Cd34* [45]. This is likely due to their relative lack of buoyancy. These studies also revealed a population of ThyAds expressing a highly metabolically active transcription program similar to beige adipose cells, termed 'ThyAd Ib'. These nuclei were differentiated by significant expression of *Ucp1*, *Ppara* and *Esrrg*. , hallmarks of beige and brown adipocytes. *Esrrg* for example encodes an orphan nuclear receptor expressed in metabolically active tissues (e.g., brain, heart, skeletal muscle, BAT) that promotes adipocyte beiging by activating mitochondrial biogenesis and oxidative metabolism [24]. *Ppara* encodes a nuclear receptor associated with metabolically active tissues such as heart and brown adipose tissue (BAT) that oxidize fatty acids at a high rate [46]. *Ppara* is also expressed in hepatocytes, where it promotes fatty acid oxidation and ketogenesis during fasting [47,48]. In combination with PPARγ, PPARα can induce beiging of white adipose tissue [49]. *Cidea*, which can be induced by the combined expression of PPARγ and PPARα and encodes a transcription coregulator that activates *Ucp1* expression [25]. *Prdm16* and *Ucp1* expression are also hallmarks of BAT [28]. PRDM16 represses type-1 interferon signaling in adipocytes which promotes thermogenic programming [50].

Interestingly however, these nuclei did not strongly express other genes associated with beige adipocyte gene expression programs, e.g. *Tbx1*, *Shox2*, *Tmem26*, or *Hoxc9*, indicating that ThyAd Ib may be distinct from previously defined populations of beige adipocytes. An intermediate population – 'ThyAd Ia' – shared expression of beige/brown genes with ThyAd Ib such as *Ppara* and *Prdm16* but with little expression of *Ucp1*. DEG analysis of ThyAd clusters alone identified *Acsl1*, *Prkr2b* and *Mecom* among the topmost ThyAd Ia-enriched genes. The products of these genes are known to positively regulate adipogenesis and FA metabolism within BAT [51-53]. ThyAd IIs displayed differential expression of genes such as *Col15a1*, *Prr16*, and *Pbx1*. These genes are often associated with EMT and ECM remodeling [54-57]. EMT has been associated with more plastic and stem-like states, allowing de-differentiation and developmental plasticity, including the ability to transition to adipocytes [58]. Within the thymus, age-associated TECs (aaTECs) are also associated with limited EMT signatures [27].

Analysis of transcription factor motifs enriched in open ThyAd chromatin supports the finding of two broad transcriptional ThyAd I and II programs and identifies potential regulators that may differentially regulate the two populations. Motif sequences for Esrrg, Ebf2 and Nr4a2 were highly enriched in ThyAd I, consistent with their significant expression in this population and roles in maintaining a beige-like transcription profile [12,24,59,60]. Both Ebf2 and Esrrg have been demonstrated to promote and maintain a beige/brown transcriptional program [24,61,62]. Esrrg

308 accessibility was mostly restricted to ThyAd Ib in both male and female mice, suggesting Esrrg
309 plays an important role in ThyAd Ib's beige-like transcriptional state. Though *Ebf2* was expressed
310 highly in all clusters, chromatin accessibility displayed a gradient pattern with higher accessibility
311 in ThyAd Is and lower accessibility in ThyAd IIs. Interestingly, though Plagl1 motif accessibility
312 was enriched in ThyAd Is, its expression by RNAseq was increased in ThyAd IIs.

313 ThyAd IIs instead showed increased accessibility for WT1, KLF12, and KLF1. WT1 is
314 known to negatively regulate thermogenic gene expression and beige fat identity [63]. WT1 also
315 modulates EMT/MET during development [64,65]. Interestingly, ThyAd II showed the strongest
316 enrichment for Foxn1 motifs, which were not detected within the RNAseq. This is consistent with
317 a model in which Foxn1 may have been expressed earlier in the etiology of ThyAd II. The origin
318 of adipocytes within the thymic compartment is not well understood. Adipogenesis involves
319 several tightly regulated steps, including the upregulation of PPARγ, a transcriptional factor
320 required for activation of downstream genes [66]. Aire-expressing TECs can give rise to "mimetic"
321 cells that adopt characteristics of peripheral cells including antigens that would not otherwise be
322 found in the thymus. These cells aid in thymic selection and the generation of central tolerance
323 [67]. In humans, Aire deficiency has been associated with Plin-1 autoreactivity and autoimmune
324 adipose infiltration [68,69]. Prior work has identified adipogenic potential in the thymic SVF [70]. These
325 findings suggest that at least a subset of the identified ThyAds may represent an uncharacterized
326 depot of mimetic cells that eluded identification due to their buoyancy. Within the thymus,
327 adipocytes have been suggested to arise from multiple sources, such as infiltration via proximity
328 to the PVS or transdifferentiation from stromal cells with adipogenic potential [71,72]. Lineage tracing
329 experiments using LacZ reporters indicate that at least some adipocytes are derived from Foxn1-
330 expressing TECs [70]. We found that differentially open chromatin in WAT-like ThyAd II nuclei are
331 enriched in binding sites for Foxn1, suggesting that this specific population may emerge from
332 TECs. Other populations Foxn1-negative, EpCAM-negative stromal cells have been identified
333 with adipogenic potential [73]. Together with our findings of multiple distinct ThyAd populations,
334 these findings are most consistent with a complex etiology for ThyAds.

335 We used confocal imaging to identify UCP1+ cells within the thymic parenchyma. These
336 cells were sparse and well-spaced and mostly confined to cortical regions. These findings are
337 consistent with work from Langhi et al., who identified several lipid-laden, Plin1+ populations
338 including preadipocytes, brown adipocytes (UCP1+), macrophages (Iba1+), and pericytes (Ng2+)
339 within the thymic parenchyma, surrounding blood vessels, and the subcapsular zone [22].

340 Thymocyte maturation is dependent on cellular crosstalk within the thymic
341 microenvironment, including between thymic stromal cells and thymocytes. For example, TECs
342 and fibroblasts secrete factors (e.g., IL-7, SCF, DLL4) that drive thymocyte
343 proliferation/differentiation [74]. Reciprocally, thymocytes provide TEC differentiation signals (e.g.,
344 RANKL, CD40, LTβ) to maintain thymic architecture [1]. TEC-derived cells in the thymus are known
345 to play additional roles beyond antigen presentation [75]. More work is required to define ThyAd
346 functions in antigen presentation and other functions such as providing trophic or metabolic
347 support to thymocytes or TECs. Similarly, although ThyAds expand with age their role in thymic
348 involution remains incompletely understood. Injection of T cell progenitors from young mice into
349 aged thymi fails to rescue declining thymopoiesis. Conversely, transplantation of fetal thymic
350 lobes into 18-month-old RAG1$^{-/-}$ mice restores host thymocyte counts to that of 6-8 week-old mice
351 [76]. The fact that other strategies, such as injection of fetal TECs or ectopic expression of Foxn1
352 within adult TECs, only partially rescues aged thymi indicates that multiple attributes intrinsic to
353 aged thymi are responsible for loss of T cell output [77-79]. The possible contribution of one of more
354 ThyAd subsets to this process also awaits experimentation.
355
356 **Limitations of the study**
357 Our findings identify heterogeneity in ThyAds and identify beige-like cells expressing UCP1 within
358 the thymic parenchyma. Although we confined the study to relatively young mice to reduce
359 accumulation of epicardial/perithymic fat which could confound the study, and although thymi
360 were extensively cleaned of fat outside the capsule before processing, it remains formally possible
361 that one or more of the ThyAd subclusters could reflect contamination from perithymic fat, which
362 is known to harbor beige-like cells. It is also possible that one or more subclusters could be
363 molecularly indistinguishable from perithymic fat. Although prior lineage tracing work pinpoints
364 TECs as a source for at least some ThyAds, and although our work is consistent with a TEC origin
365 for ThyAd II, this has not been formally demonstrated. Finally, the study is intended to provide the
366 first molecular ThyAd atlas, and as such contains no information of the functions for these cells in
367 T cell development or thymic involution.

368 **METHOD DETAILS**

369 **Laboratory mice**

370 All mice were C57BL/6J background (#000664, Jackson Laboratories, Bar Harbor, Maine, USA).
371 Mice were housed on a 12h dark/light cycle in groups (maximum five mice per cage) with ad
372 libitum access to water and standard chow diet. All procedures were performed in accordance
373 with the University of Utah Institutional Animal Care and Use Committee (Protocol #00001553).
374

375 **ThyAd isolation**

376 Intact thymi were quickly removed and transferred to a petri dish on ice with ~300uL PBS to keep
377 tissue moist. Thymic capsules were cleaned of directly attached perithymic fat and connective
378 tissues, rinsed a final time with PBS, and transferred to a 15mL conical tube. Digestion Buffer
379 (1mM CaCl2, 250mM sucrose, 1.5mM MgCl2, 10mM KCl, 15mM HEPES, 0.1% BSA) with DNase
380 I (8 μg/mL, D513, Sigma Aldrich) and Collagenase II (2 mg/mL, C1764, Sigma Aldrich) in DMEM-
381 F12 10% FBS was added to each sample and thymi were digested for approximately 10-15
382 minutes at 37°C, horizontally on a shaker set at 300 rpm. Once most of the thymic tissue was
383 digested, an equal volume of FBS was added to each sample to quench the reaction, mixed by
384 gentle pipetting. Samples were fractionated by an initial centrifugation at 300 × *g* at 4°C. The
385 topmost white layer containing mature, floating adipocytes was transferred to a clean 15 mL tube
386 (Figure 1). Then, 10 mL of Wash Buffer (DMEM-F12, 15mM HEPES, 10% FBS) were added to
387 each sample and mixed by gentle inversion and/or trituration with a micropipette to prevent
388 bursting of the adipocytes. Samples were left on ice for 10 min, followed by a second round of
389 centrifugation at 150 × *g* at 4°C. The white floating layer was transferred to a 5 mL conical tube
390 and washed with 4 mL Wash Buffer. Samples were left on ice for 10 min, and spun at 150 × *g* at
391 4°C. The floating fraction was collected and transferred to a clean 1.5 mL eppendorf tube. Without
392 adding more media, samples were centrifuged at 150 *x g* at 4°C. Residual buffer was carefully
393 removed from the bottom of the tube with a 5 mL syringe and 21-gage needle. The remaining
394 white layer of packed adipocytes was transferred to a clean, prechilled 1.5 mL eppendorf tube for
395 nuclei isolation. For the data shown in Figure 4, 6 male thymi were collected, combined, and
396 processed similarly. Gonadal (inguinal) fat (gWAT) was prepared from the same mice in parallel
397 as a quality control.
398

399 **Nuclei and 10X library preparation**

400 To isolate nuclei, samples were incubated with 100 μL 0.1x lysis buffer for 3-5 min on ice as
401 previously described (10X Genomics, Demonstrated Protocol CG000366 Rev D). After washing
402 and centrifugation following the outlined protocol, nuclei were resuspended in diluted 1x Nuclei
403 Buffer (10X Genomics, PN 2000207). The concentration of nuclei was determined by AO/PI using
404 a Luna-FL (Logos Biosystems, Inc., Gyeonggi-do, Korea). Approximately 5,000 nuclei were
405 immediately loaded onto a 10X Next GEM Chip J (10X Genomics, PN 1000230). Single-nuclei
406 libraries were prepared using Chromium Next GEM Single Cell Multiome Reagent Kit A reagents
407 (10X Genomics, PN 1000284) and assessed for quality using an Agilent D1000 ScreenTape.
408 Libraries were sequenced on an Illumina NovaSeq X instrument targeting 100 million paired end
409 reads (GEX) and 300 million paired end reads (ATAC) of 150 bp for each sample.
410
411 **Data analysis**
412 For female thymi, reads were aligned to the *mm10* reference genome (package 2020-A) to
413 generate feature-barcode matrices using cellranger (version 2.0.2). After quality control and
414 thresholding of cellranger output matrices, normalization and PCA of 3,610 high-quality single
415 nuclei was performed in Seurat (v5.1.0) [80]. Sample quality was assessed by joint RNAseq and
416 ATACseq quality control parameters as described in the Seurat WNN and Signac 10x multiomic
417 analysis vignettes [80,81]. Briefly, high-quality nuclei were defined by the number of ATAC transcripts
418 (nCount_ATAC >500 & <70,000), unique genes (nFeature_RNA >200 & <2,500), mitochondrial
419 mRNA content (mt.percent_RNA <20%), nucleosome signal (<2), and TSS enrichment (>1). 3,610
420 nuclei were recovered using this method. Utilizing the Seurat SCTransform pipeline, dimensional
421 reduction (PCA) was performed on the top 3,000 most variable genes. Equivalent normalization
422 of the ATACseq data was performed by latent semantic indexing (LSI). A 'weighted nearest
423 neighbor' (WNN) UMAP was generated using the FindMultiModalNeighbors function, taking both
424 RNAseq and ATACseq datasets into account for subsequent UMAP and cluster visualization.
425 Ptprc-enriched clusters were identified and excluded from downstream analyses while ThyAds
426 were identified as $Ptprc^{lo}$. This operation yielded 429 remaining nuclei. Adipocytes were
427 reclustered using the SCTransform pipeline. Differential gene expression between the newly
428 defined clusters was determined by applying the FindAllMarkers or FindMarkers function, which
429 use a non-parametric Wilcoxon rank sum test with Bonferroni correction on all normalized
430 features. For applicable figures, levels of significance are denoted as *$p < 0.05$, **$p < 0.01$, ***$p <$
431 0.001, and ****$p < 0.0001$

For male thymi, 4,342 thymic and 4,968 gWAT nuclei were identified in each sample, and following removal of Ptprc-expressing cells 1,521 filtered ThyAd nuclei and 3,806 filtered gWAT nuclei were present.

Motif, transcription factor, and GO analysis

Motif analysis was performed using chromVAR and additional packages as outlined in the Signac motif analysis and Seurat WNN vignettes [81]. Clusters were compared against each other to identify the topmost differentially accessible motifs (p.val <0.05). To identify transcription factors (TFs) which may underlie ThyAd cluster transcriptional state, TFs with both high differential expression and their corresponding accessible motifs were determined using Seurat's 'presto' package, which uses a Wilcox rank sum test to calculate p-values for both datasets and returning only TFs with p.val <0.01. GO analysis was performed on ThyAd I and ThyAd II cluster DEGs with adjusted p.val <0.05 using the 'fgsea' R package for Biological Process and Hallmark gene sets [82].

Immunofluorescence and confocal microscopy

6-month old mice were euthanized by isofluorane and perfused with PBS. Intact thymi and directly attached connective tissue were carefully removed, washed in PBS, and postfixed for 30 min in 4% (w/v) paraformaldehyde (PFA). After 3x PBS washes for 20 min each, thymi were incubated in 10% sucrose for 1 hr and then left in 20% sucrose overnight at 4°C. The following day, thymi were incubated in a series of 30% sucrose for at least 2 hr, then incubated in 2:1 OCT compound:20% sucrose for 1 hr. Tissue was embedded in 100% OCT over a dry ice and 2-propanol slurry for sectioning. 10-20 μm cryosections were dried for 40-60 min at 37°C and rehydrated in cold PBS. Tissue was rinsed 3x in PBST (0.1% Tween 20), and permeabilized in PBST for 15 min. Detergent was removed by rinsing 3x in PBS, following which samples were incubated in prewarmed 0.5-1X TrueBlack Lipofluscin Autofluorescence Quencher (Biotium, Fremont, CA) for 2 min. Slides were blocked for 1 hr at RT in PBS containing 10% normal donkey serum, 5% BSA, and 0.2% Triton-X, and incubated overnight in a primary antibody cocktail (10% donkey normal serum, 5% BSA) containing rabbit anti-UCP1 or rabbit anti-PPARγ (Cell Signaling Technologies, MA, USA) at 4°C. Sections were washed in PBS for 20 min thrice, followed by a 2 hr incubation with a secondary buffer cocktail at RT (1% BSA, 1:2000 Hoescht 33342, Thermo Fischer Scientific H3570) with or without donkey anti-Alexa Fluor 647 nm (1:400, Invitrogen, La

464 Jolla, CA, USA). Slides were washed and mounted with Fluoromount-G (Thermo Fischer
465 Scientific 00-4958). If substantial TrueBlack was removed from slides after incubation with
466 blocking buffer, the post-staining treatment protocol was used per manufacturer's protocol.
467 Stained sections were imaged by resonance scanning confocal microscopy (A1R confocal system
468 and Eclipse Ti inverted microscope; Nikon, Melville, NY, USA) with a 20X objective and 3X or 8X
469 optical zoom (0.41μm/px).

AUTHOR CONTRIBUTIONS

N.J.S. and D.T. conceived the study. KEV helped with generation of the ThyAd isolation protocol. N.J.S. and A.F. performed experiments. N.J.S. analyzed the data and generated figures. All authors contributed to the writing of the manuscript.

ACKNOWLEDGEMENTS

We thank W-L Lo for critical reading of the manuscript. We thank M. Chandrashekharan for help with graphics. We thank B. Dalley, O. Allen and the University of Utah Huntsman Cancer Institute High-Throughput Genomics Core Facility. This work was supported by a pilot grant from the University of Utah Center Diabetes and Metabolism Research Center (DMRC) to DT.

DECLARATION OF INTERESTS

The authors declare no competing interests.

483 **FIGURE LEGENDS**

484 **Figure 1. Female ThyAds are heterogeneous, with one subclustered harboring**
485 **transcriptional signatures of metabolically active beige fat.**

486 (A) Experimental design for isolation and multiomic sequencing of murine ThyAds. Thymi were
487 processed by mechanical disaggregation, digestion, centrifugation (isolation by buoyancy) and
488 nuclei isolation prior to single-nucleus ATACseq + RNAseq multiomics.

489 (B) Example thymus prior to and after removal of perithymic fat. The septa and thymic lobes were
490 kept intact such that the fatty tissue between the lobes is retained.

491 (C) UMAP projection and clustering of ThyAds by RNAseq, ATACseq, and Weighted Next
492 Neighbor (WNN) analysis. ThyAds (n = 429, avg gene count 2,974) were reclustered after removal
493 of Prprc-expressing nuclei. A residual Ptprc+ cluster was also present.

494 (D) Expression of most distinguishing ThyAd marker genes by cluster. A heatmap displaying the
495 top 10 DEGs within each ThyAd subpopulation is shown.

496

497 **Figure 2. ThyAd I and II display highly differential gene expression.**

498 (A) Violin plots highlighting differential and shared expression of ThyAd I and II cluster-defining
499 genes. Recolored UMAP denotes superclusters Ia/b and Ia/b/c are shown at right.

500 (B) GO Biological Process Analysis for ThyAd Is and II superclusters.

501

502 **Figure 3. Differentially accessible chromatin and transcription factor motif enrichment in**
503 **different ThyAd subpopulations.**

504 (A) Single-nucleus ATAC-seq open chromatin genome tracks at the *Ppara*, *Cidea* and *Ucp1* loci
505 are shown for each subpopulation.

506 (B) Motif analysis comparing combined ThyAd I and II subpopulations. The top 6 most enriched
507 motifs are shown for each grouped population. Asterisks denote motifs unique to that population.

508

509 **Figure 4. Male murine ThyAds are heterogenous and transcriptionally distinct from gWAT.**

510 (A) Experimental design for isolation and multiomic sequencing of murine ThyAds.

511 (B) Single-nucleus RNA-seq UMAPs comparing ThyAds with gWAT isolated from 4-month-old
512 male mice. Nuclei were labeled by tissue.

513 (C) Feature plots showing expression of selected marker genes *Ptprc*, *Pparg*, *Fabp4*, *Adipoq*,
514 *Ppara*, and *Esrrg*.

515 (D) ThyAds were reclustered alone to distinguish 1a, Ib, IIa, IIb, and IIc populations. UMAP feature
516 plots are shown for *Ppara*, *Ghr*, *Ppargc1b*, *Pparg*, *Fabp4*, *Fgf14*, and *Esrrg*.
517
518 **Figure 5. UCP1^{+} cells are detectable in the thymic cortical regions of 6-month-old female**
519 **mice.**
520 (A) Top: 0.8 μm confocal Z-stack images of UCP1 immunofluorescence-stained cryosections of
521 a region of a 6-month-old female murine thymus where the cortex meets the capsule. Slides were
522 counterstained with Hoescht. Dense nuclear stain (blue) denotes the thymic parenchyma,
523 predominantly TECs and thymocytes. Intense UCP1 staining is present in perithymic fat attached
524 to the thymic capsule with a distinct expression pattern compared to scattered parenchymal
525 UCP1+ cells (highlighted with yellow arrows). At right is shown a higher magnification image of
526 the same slide. Bottom: an adjacent cryosection stained and imaged identically except lacking
527 the primary antibody.
528 (B) Similarly processed images of a different section from the same thymus.
529
530 **SUPPLEMENTAL FIGURE LEGENDS**
531 **Supplemental Figure 1. Quality control for single-nucleus ATAC-seq plus RNA-seq**
532 **multiomics.**
533 (A) example nuclei following isolation. Areas of heterochromatin are preserved.
534 (B) Thresholding and quality control parameters employed to eliminate low-quality nuclei. Left:
535 mitochondrial regression/normalization. Removed nuclei are shown in gray (top left). Right:
536 Density plot showing retained nuclei by TSS enrichment and total peak fragments. nCount_ATAC
537 quantiles are: 5% 6438.45; 10% 7834; 90% 29520.1. TSS. Enrichment quantiles are: 5% 5.47;
538 10% 5.8; 95% 8.96.
539 (C) WNN UMAP clustering of 3,610 nuclei isolated from the floating fraction of female 6-month
540 old thymic tissue. Clusters 3 and 10 are highlighted (red circles) and identified as Ptprc^{lo} and
541 Pparg^{+}Plin1^{+}. This subset was used for further downstream analysis.
542 (D) Selected marker genes used to identify immune populations and adipocytes are shown as
543 violin plots by cluster.
544
545 **Supplemental Figure 2. Lipid-metabolism-related gene expression comparing whole**
546 **sample and ThyAds.**

547 (A) Dot Plots of whole sample ThyAds showing expression of genes associated with lipid
548 metabolism. Genes associated with lipogenesis (*Fasn*, *Acaca*, *Elovl6*, *Dgat1*, *Dgat2*, *Srebf1*, *Acly*,
549 *Scd1*, *Scd1*) and lipolysis (*Lipe*, *Pnpla2*, *Mgll*, *Gk*, *Abhd5*) are shown.
550 (B) The same analysis was performed for subsetted Pparg+Fabp4+Plin1+ ThyAds and the
551 residual Ptprc+ cluster.
552
553 **Supplemental Figure 3. Expression of selected markers by ThyAds and top DEGs by**
554 **cluster.**
555 (A) Heatmap displaying the top 10 DEGs for cluster including the Ptprc+ nuclei.
556 (B) WNN UMAP projections of genes encoding selected adipokines (*Adipoq*, *Retn*, *Lep*, *Cfd*) and
557 beige/brown adipocyte marker genes (*Cidea*, *Prdm16*, *Ucp1*, *Esrrg*, *Ppargc1a*, *Ppargc1b*). *Plin1*,
558 *Fasn*, *Ebf2*, *Zfp423*, *Col15a1*, *Aldh1a1*, *Prr16* and *Rems3* are also shown.
559
560 **Supplemental Figure 4. Gene expression and open chromatin states of potential ThyAd**
561 **transcription regulators.**
562 (A) Feature plots of WNN UMAPS showing expression and chromatin accessibility for additional
563 genes. *Ebf2*, *Esrrg*, *Plagl1*, and *Foxn1* are shown. Gene expression plots for *Foxn1* could not be
564 generated because Foxn1 was not expressed in any nucleus. The WNN plot from Figure 1C is
565 recapitulated at right for comparison.
566 (B) Single-nucleus ATAC-seq open chromatin genome tracks at the *Foxn1* locus is shown for
567 each subpopulation.
568
569 **Supplemental Figure 5. Gene expression differences associated with ThyAd and gWAT**
570 **tissue from 4-month-old male mice.**
571 (A) Heatmap displaying the top 10 DEGs within each ThyAd and gWAT subpopulation is shown.
572 (B) Similar to Figure 4C except additional genes are shown: *Ebf2*, *Cidea*, *Prdm16*, *Ghr*, *Ebf1*, and
573 *Aifm2*.
574
575 **Supplemental Figure 6. PPARγ-positive cells identified within the thymus.**
576 IF image of a 16 μm cryosection of a thymus from a 6-month-old female mouse. Samples was
577 stained with BODIPY (488 nm), rabbit anti-PPARγ (647 nm) and Hoescht (405 nm).

578 **REFERENCES**

579 1. Li, Y.R., and Zuniga-Pflucker, J.C. (2023). Thymus aging and immune reconstitution,
580 progresses and challenges. Semin Immunol *70*, 101837. 10.1016/j.smim.2023.101837.
581 2. Lynch, H.E., Goldberg, G.L., Chidgey, A., Van den Brink, M.R., Boyd, R., and
582 Sempowski, G.D. (2009). Thymic involution and immune reconstitution. Trends Immunol
583 *30*, 366-373. 10.1016/j.it.2009.04.003.
584 3. Min, H., Montecino-Rodriguez, E., and Dorshkind, K. (2004). Reduction in the
585 developmental potential of intrathymic T cell progenitors with age. J Immunol *173*, 245-
586 250. 10.4049/jimmunol.173.1.245.
587 4. Cisneros, B., Garcia-Aguirre, I., Unzueta, J., Arrieta-Cruz, I., Gonzalez-Morales, O.,
588 Dominguez-Larrieta, J.M., Tamez-Gonzalez, A., Leyva-Gomez, G., and Magana, J.J.
589 (2022). Immune system modulation in aging: Molecular mechanisms and therapeutic
590 targets. Front Immunol *13*, 1059173. 10.3389/fimmu.2022.1059173.
591 5. Weng, N.P., Akbar, A.N., and Goronzy, J. (2009). CD28(-) T cells: their role in the age-
592 associated decline of immune function. Trends Immunol *30*, 306-312.
593 10.1016/j.it.2009.03.013.
594 6. Saurwein-Teissl, M., Lung, T.L., Marx, F., Gschosser, C., Asch, E., Blasko, I., Parson,
595 W., Bock, G., Schonitzer, D., Trannoy, E., and Grubeck-Loebenstein, B. (2002). Lack of
596 antibody production following immunization in old age: association with CD8(+)CD28(-) T
597 cell clonal expansions and an imbalance in the production of Th1 and Th2 cytokines. J
598 Immunol *168*, 5893-5899. 10.4049/jimmunol.168.11.5893.
599 7. Dorshkind, K., and Swain, S. (2009). Age-associated declines in immune system
600 development and function: causes, consequences, and reversal. Curr Opin Immunol *21*,
601 404-407. 10.1016/j.coi.2009.07.001.
602 8. Youm, Y.H., Yang, H., Amin, R., Smith, S.R., Leff, T., and Dixit, V.D. (2010).
603 Thiazolidinedione treatment and constitutive-PPARgamma activation induces ectopic
604 adipogenesis and promotes age-related thymic involution. Aging Cell *9*, 478-489.
605 10.1111/j.1474-9726.2010.00574.x.
606 9. Laan, M., Haljasorg, U., Kisand, K., Salumets, A., and Peterson, P. (2016). Pregnancy-
607 induced thymic involution is associated with suppression of chemokines essential for T-
608 lymphoid progenitor homing. Eur J Immunol *46*, 2008-2017. 10.1002/eji.201646309.
609 10. Billard, M.J., Gruver, A.L., and Sempowski, G.D. (2011). Acute endotoxin-induced
610 thymic atrophy is characterized by intrathymic inflammatory and wound healing
611 responses. PLoS One *6*, e17940. 10.1371/journal.pone.0017940.
612 11. Howard, J.K., Lord, G.M., Matarese, G., Vendetti, S., Ghatei, M.A., Ritter, M.A., Lechler,
613 R.I., and Bloom, S.R. (1999). Leptin protects mice from starvation-induced lymphoid
614 atrophy and increases thymic cellularity in ob/ob mice. J Clin Invest *104*, 1051-1059.
615 10.1172/JCI6762.
616 12. Emont, M.P., Jacobs, C., Essene, A.L., Pant, D., Tenen, D., Colleluori, G., Di Vincenzo,
617 A., Jorgensen, A.M., Dashti, H., Stefek, A., et al. (2022). A single-cell atlas of human and
618 mouse white adipose tissue. Nature *603*, 926-933. 10.1038/s41586-022-04518-2.
619 13. Bautista, J.L., Cramer, N.T., Miller, C.N., Chavez, J., Berrios, D.I., Byrnes, L.E.,
620 Germino, J., Ntranos, V., Sneddon, J.B., Burt, T.D., et al. (2021). Single-cell
621 transcriptional profiling of human thymic stroma uncovers novel cellular heterogeneity in
622 the thymic medulla. Nat Commun *12*, 1096. 10.1038/s41467-021-21346-6.
623 14. Cordes, M., Cante-Barrett, K., van den Akker, E.B., Moretti, F.A., Kielbasa, S.M.,
624 Vloemans, S.A., Garcia-Perez, L., Teodosio, C., van Dongen, J.J.M., Pike-Overzet, K.,
625 et al. (2022). Single-cell immune profiling reveals thymus-seeding populations, T cell

626 commitment, and multilineage development in the human thymus. Sci Immunol *7*,
627 eade0182. 10.1126/sciimmunol.ade0182.
628 15. Lavaert, M., Liang, K.L., Vandamme, N., Park, J.E., Roels, J., Kowalczyk, M.S., Li, B.,
629 Ashenberg, O., Tabaka, M., Dionne, D., et al. (2020). Integrated scRNA-Seq Identifies
630 Human Postnatal Thymus Seeding Progenitors and Regulatory Dynamics of
631 Differentiating Immature Thymocytes. Immunity *52*, 1088-1104 e1086.
632 10.1016/j.immuni.2020.03.019.
633 16. Le, J., Park, J.E., Ha, V.L., Luong, A., Branciamore, S., Rodin, A.S., Gogoshin, G., Li, F.,
634 Loh, Y.E., Camacho, V., et al. (2020). Single-Cell RNA-Seq Mapping of Human
635 Thymopoiesis Reveals Lineage Specification Trajectories and a Commitment Spectrum
636 in T Cell Development. Immunity *52*, 1105-1118 e1109. 10.1016/j.immuni.2020.05.010.
637 17. Gabriely, I., Ma, X.H., Yang, X.M., Atzmon, G., Rajala, M.W., Berg, A.H., Scherer, P.,
638 Rossetti, L., and Barzilai, N. (2002). Removal of visceral fat prevents insulin resistance
639 and glucose intolerance of aging: an adipokine-mediated process? Diabetes *51*, 2951-
640 2958. 10.2337/diabetes.51.10.2951.
641 18. Huh, J.Y., Park, J., Kim, J.I., Park, Y.J., Lee, Y.K., and Kim, J.B. (2017). Deletion of
642 CD1d in Adipocytes Aggravates Adipose Tissue Inflammation and Insulin Resistance in
643 Obesity. Diabetes *66*, 835-847. 10.2337/db16-1122.
644 19. Zoico, E., Rubele, S., De Caro, A., Nori, N., Mazzali, G., Fantin, F., Rossi, A., and
645 Zamboni, M. (2019). Brown and Beige Adipose Tissue and Aging. Front Endocrinol
646 (Lausanne) *10*, 368. 10.3389/fendo.2019.00368.
647 20. Porter, J.W., Barnas, J.L., Welly, R., Spencer, N., Pitt, J., Vieira-Potter, V.J., and
648 Kanaley, J.A. (2020). Age, Sex, and Depot-Specific Differences in Adipose-Tissue
649 Estrogen Receptors in Individuals with Obesity. Obesity (Silver Spring) *28*, 1698-1707.
650 10.1002/oby.22888.
651 21. Varghese, M., Song, J., and Singer, K. (2021). Age and Sex: Impact on adipose tissue
652 metabolism and inflammation. Mech Ageing Dev *199*, 111563.
653 10.1016/j.mad.2021.111563.
654 22. Langhi, L.G., Andrade, L.R., Shimabukuro, M.K., van Ewijk, W., Taub, D.D., Borojevic,
655 R., and de Mello Coelho, V. (2015). Lipid-Laden Multilocular Cells in the Aging Thymus
656 Are Phenotypically Heterogeneous. PLoS One *10*, e0141516.
657 10.1371/journal.pone.0141516.
658 23. Dixen, K., Basse, A.L., Murholm, M., Isidor, M.S., Hansen, L.H., Petersen, M.C.,
659 Madsen, L., Petrovic, N., Nedergaard, J., Quistorff, B., and Hansen, J.B. (2013).
660 ERRgamma enhances UCP1 expression and fatty acid oxidation in brown adipocytes.
661 Obesity (Silver Spring) *21*, 516-524. 10.1002/oby.20067.
662 24. Muller, S., Perdikari, A., Dapito, D.H., Sun, W., Wollscheid, B., Balaz, M., and Wolfrum,
663 C. (2020). ESRRG and PERM1 Govern Mitochondrial Conversion in Brite/Beige
664 Adipocyte Formation. Front Endocrinol (Lausanne) *11*, 387. 10.3389/fendo.2020.00387.
665 25. Jash, S., Banerjee, S., Lee, M.J., Farmer, S.R., and Puri, V. (2019). CIDEA
666 Transcriptionally Regulates UCP1 for Britening and Thermogenesis in Human Fat Cells.
667 iScience *20*, 73-89. 10.1016/j.isci.2019.09.011.
668 26. Montoya, M., and Del Val, M. (1999). Intracellular rate-limiting steps in MHC class I
669 antigen processing. J Immunol *163*, 1914-1922.
670 27. Kousa, A.I., Jahn, L., Zhao, K., Flores, A.E., Acenas, D., 2nd, Lederer, E., Argyropoulos,
671 K.V., Lemarquis, A.L., Granadier, D., Cooper, K., et al. (2024). Age-related epithelial
672 defects limit thymic function and regeneration. Nat Immunol *25*, 1593-1606.
673 10.1038/s41590-024-01915-9.

674 28. Seale, P., Kajimura, S., Yang, W., Chin, S., Rohas, L.M., Uldry, M., Tavernier, G.,
675 Langin, D., and Spiegelman, B.M. (2007). Transcriptional control of brown fat
676 determination by PRDM16. Cell Metab *6*, 38-54. 10.1016/j.cmet.2007.06.001.
677 29. Hinds, T.D., Jr., Kipp, Z.A., Xu, M., Yiannikouris, F.B., Morris, A.J., Stec, D.F., Wahli, W.,
678 and Stec, D.E. (2021). Adipose-Specific PPARalpha Knockout Mice Have Increased
679 Lipogenesis by PASK-SREBP1 Signaling and a Polarity Shift to Inflammatory
680 Macrophages in White Adipose Tissue. Cells *11*. 10.3390/cells11010004.
681 30. Holman, C.D., Sakers, A.P., Calhoun, R.P., Cheng, L., Fein, E.C., Jacobs, C., Tsai, L.,
682 Rosen, E.D., and Seale, P. (2024). Aging impairs cold-induced beige adipogenesis and
683 adipocyte metabolic reprogramming. bioRxiv. 10.1101/2023.03.20.533514.
684 31. Kim, K.H., Lee, K., Moon, Y.S., and Sul, H.S. (2001). A cysteine-rich adipose tissue-
685 specific secretory factor inhibits adipocyte differentiation. J Biol Chem *276*, 11252-
686 11256. 10.1074/jbc.C100028200.
687 32. Nehls, M., Kyewski, B., Messerle, M., Waldschutz, R., Schuddekopf, K., Smith, A.J., and
688 Boehm, T. (1996). Two genetically separable steps in the differentiation of thymic
689 epithelium. Science *272*, 886-889. 10.1126/science.272.5263.886.
690 33. Simpson, J.G., Gray, E.S., and Beck, J.S. (1975). Age involution in the normal human
691 adult thymus. Clin Exp Immunol *19*, 261-265.
692 34. Pido-Lopez, J., Imami, N., and Aspinall, R. (2001). Both age and gender affect thymic
693 output: more recent thymic migrants in females than males as they age. Clin Exp
694 Immunol *125*, 409-413. 10.1046/j.1365-2249.2001.01640.x.
695 35. Sandstedt, M., Chung, R.W.S., Skoglund, C., Lundberg, A.K., Ostgren, C.J., Ernerudh,
696 J., and Jonasson, L. (2023). Complete fatty degeneration of thymus associates with
697 male sex, obesity and loss of circulating naive CD8(+) T cells in a Swedish middle-aged
698 population. Immun Ageing *20*, 45. 10.1186/s12979-023-00371-7.
699 36. Baran-Gale, J., Morgan, M.D., Maio, S., Dhalla, F., Calvo-Asensio, I., Deadman, M.E.,
700 Handel, A.E., Maynard, A., Chen, S., Green, F., et al. (2020). Ageing compromises
701 mouse thymus function and remodels epithelial cell differentiation. Elife *9*.
702 10.7554/eLife.56221.
703 37. Flores, K.G., Li, J., Sempowski, G.D., Haynes, B.F., and Hale, L.P. (1999). Analysis of
704 the human thymic perivascular space during aging. J Clin Invest *104*, 1031-1039.
705 10.1172/JCI7558.
706 38. Kumar, R., Langer, J.C., and Snoeck, H.W. (2006). Transforming growth factor-beta2 is
707 involved in quantitative genetic variation in thymic involution. Blood *107*, 1974-1979.
708 10.1182/blood-2005-04-1495.
709 39. Frontini, A., Rousset, S., Cassard-Doulcier, A.M., Zingaretti, C., Ricquier, D., and Cinti,
710 S. (2007). Thymus uncoupling protein 1 is exclusive to typical brown adipocytes and is
711 not found in thymocytes. J Histochem Cytochem *55*, 183-189. 10.1369/jhc.6A7013.2006.
712 40. Aw, D., Silva, A.B., Maddick, M., von Zglinicki, T., and Palmer, D.B. (2008). Architectural
713 changes in the thymus of aging mice. Aging Cell *7*, 158-167. 10.1111/j.1474-
714 9726.2007.00365.x.
715 41. Angueira, A.R., Sakers, A.P., Holman, C.D., Cheng, L., Arbocco, M.N., Shamsi, F.,
716 Lynes, M.D., Shrestha, R., Okada, C., Batmanov, K., et al. (2021). Defining the lineage
717 of thermogenic perivascular adipose tissue. Nat Metab *3*, 469-484. 10.1038/s42255-021-
718 00380-0.
719 42. Shao, M., Hepler, C., Vishvanath, L., MacPherson, K.A., Busbuso, N.C., and Gupta,
720 R.K. (2017). Fetal development of subcutaneous white adipose tissue is dependent on
721 Zfp423. Mol Metab *6*, 111-124. 10.1016/j.molmet.2016.11.009.

722 43. Trayhurn, P., and Wood, I.S. (2004). Adipokines: inflammation and the pleiotropic role of
723 white adipose tissue. Br J Nutr *92*, 347-355. 10.1079/bjn20041213.
724 44. Lynch, L., Nowak, M., Varghese, B., Clark, J., Hogan, A.E., Toxavidis, V., Balk, S.P.,
725 O'Shea, D., O'Farrelly, C., and Exley, M.A. (2012). Adipose tissue invariant NKT cells
726 protect against diet-induced obesity and metabolic disorder through regulatory cytokine
727 production. Immunity *37*, 574-587. 10.1016/j.immuni.2012.06.016.
728 45. Cawthorn, W.P., Scheller, E.L., and MacDougald, O.A. (2012). Adipose tissue stem cells
729 meet preadipocyte commitment: going back to the future. J Lipid Res *53*, 227-246.
730 10.1194/jlr.R021089.
731 46. Braissant, O., Foufelle, F., Scotto, C., Dauca, M., and Wahli, W. (1996). Differential
732 expression of peroxisome proliferator-activated receptors (PPARs): tissue distribution of
733 PPAR-alpha, -beta, and -gamma in the adult rat. Endocrinology *137*, 354-366.
734 10.1210/endo.137.1.8536636.
735 47. Peeters, A., and Baes, M. (2010). Role of PPARalpha in Hepatic Carbohydrate
736 Metabolism. PPAR Res *2010*. 10.1155/2010/572405.
737 48. Kersten, S., Seydoux, J., Peters, J.M., Gonzalez, F.J., Desvergne, B., and Wahli, W.
738 (1999). Peroxisome proliferator-activated receptor alpha mediates the adaptive response
739 to fasting. J Clin Invest *103*, 1489-1498. 10.1172/JCI6223.
740 49. Kroon, T., Harms, M., Maurer, S., Bonnet, L., Alexandersson, I., Lindblom, A., Ahnmark,
741 A., Nilsson, D., Gennemark, P., O'Mahony, G., et al. (2020). PPARgamma and
742 PPARalpha synergize to induce robust browning of white fat in vivo. Mol Metab *36*,
743 100964. 10.1016/j.molmet.2020.02.007.
744 50. Kissig, M., Ishibashi, J., Harms, M.J., Lim, H.W., Stine, R.R., Won, K.J., and Seale, P.
745 (2017). PRDM16 represses the type I interferon response in adipocytes to promote
746 mitochondrial and thermogenic programing. EMBO J *36*, 1528-1542.
747 10.15252/embj.201695588.
748 51. Peverelli, E., Ermetici, F., Corbetta, S., Gozzini, E., Avagliano, L., Zappa, M.A.,
749 Bulfamante, G., Beck-Peccoz, P., Spada, A., and Mantovani, G. (2013). PKA regulatory
750 subunit R2B is required for murine and human adipocyte differentiation. Endocr Connect
751 *2*, 196-207. 10.1530/EC-13-0049.
752 52. Harms, M.J., Ishibashi, J., Wang, W., Lim, H.W., Goyama, S., Sato, T., Kurokawa, M.,
753 Won, K.J., and Seale, P. (2014). Prdm16 is required for the maintenance of brown
754 adipocyte identity and function in adult mice. Cell Metab *19*, 593-604.
755 10.1016/j.cmet.2014.03.007.
756 53. Ellis, J.M., Li, L.O., Wu, P.C., Koves, T.R., Ilkayeva, O., Stevens, R.D., Watkins, S.M.,
757 Muoio, D.M., and Coleman, R.A. (2010). Adipose acyl-CoA synthetase-1 directs fatty
758 acids toward beta-oxidation and is required for cold thermogenesis. Cell Metab *12*, 53-
759 64. 10.1016/j.cmet.2010.05.012.
760 54. Kang, G.J., Park, J.H., Kim, H.J., Kim, E.J., Kim, B., Byun, H.J., Yu, L., Nguyen, T.M.,
761 Nguyen, T.H., Kim, K.S., et al. (2022). PRR16/Largen Induces Epithelial-Mesenchymal
762 Transition through the Interaction with ABI2 Leading to the Activation of ABL1 Kinase.
763 Biomol Ther (Seoul) *30*, 340-347. 10.4062/biomolther.2022.066.
764 55. Monteiro, M.C., Sanyal, M., Cleary, M.L., Sengenes, C., Bouloumie, A., Dani, C., and
765 Billon, N. (2011). PBX1: a novel stage-specific regulator of adipocyte development. Stem
766 Cells *29*, 1837-1848. 10.1002/stem.737.
767 56. Xia, T., Shen, Z., Cai, J., Pan, M., and Sun, C. (2020). ColXV Aggravates Adipocyte
768 Apoptosis by Facilitating Abnormal Extracellular Matrix Remodeling in Mice. Int J Mol Sci
769 *21*. 10.3390/ijms21030959.

770 57. Zhu, X., Wei, L., Bai, Y., Wu, S., and Han, S. (2017). FoxC1 promotes epithelial-
771 mesenchymal transition through PBX1 dependent transactivation of ZEB2 in esophageal
772 cancer. Am J Cancer Res *7*, 1642-1653.
773 58. Lambert, A.W., and Weinberg, R.A. (2021). Linking EMT programmes to normal and
774 neoplastic epithelial stem cells. Nat Rev Cancer *21*, 325-338. 10.1038/s41568-021-
775 00332-6.
776 59. Roh, H.C., Tsai, L.T.Y., Shao, M., Tenen, D., Shen, Y., Kumari, M., Lyubetskaya, A.,
777 Jacobs, C., Dawes, B., Gupta, R.K., and Rosen, E.D. (2018). Warming Induces
778 Significant Reprogramming of Beige, but Not Brown, Adipocyte Cellular Identity. Cell
779 Metab *27*, 1121-1137 e1125. 10.1016/j.cmet.2018.03.005.
780 60. Lee, S., Benvie, A.M., Park, H.G., Spektor, R., Harlan, B., Brenna, J.T., Berry, D.C., and
781 Soloway, P.D. (2022). Remodeling of gene regulatory networks underlying thermogenic
782 stimuli-induced adipose beiging. Commun Biol *5*, 584. 10.1038/s42003-022-03531-5.
783 61. Rajakumari, S., Wu, J., Ishibashi, J., Lim, H.W., Giang, A.H., Won, K.J., Reed, R.R., and
784 Seale, P. (2013). EBF2 determines and maintains brown adipocyte identity. Cell Metab
785 *17*, 562-574. 10.1016/j.cmet.2013.01.015.
786 62. Brown, E.L., Hazen, B.C., Eury, E., Wattez, J.S., Gantner, M.L., Albert, V., Chau, S.,
787 Sanchez-Alavez, M., Conti, B., and Kralli, A. (2018). Estrogen-Related Receptors
788 Mediate the Adaptive Response of Brown Adipose Tissue to Adrenergic Stimulation.
789 iScience *2*, 221-237. 10.1016/j.isci.2018.03.005.
790 63. Kirschner, K.M., Foryst-Ludwig, A., Gohlke, S., Li, C., Flores, R.E., Kintscher, U.,
791 Schupp, M., Schulz, T.J., and Scholz, H. (2022). Wt1 haploinsufficiency induces
792 browning of epididymal fat and alleviates metabolic dysfunction in mice on high-fat diet.
793 Diabetologia *65*, 528-540. 10.1007/s00125-021-05621-1.
794 64. Martinez-Estrada, O.M., Lettice, L.A., Essafi, A., Guadix, J.A., Slight, J., Velecela, V.,
795 Hall, E., Reichmann, J., Devenney, P.S., Hohenstein, P., et al. (2010). Wt1 is required
796 for cardiovascular progenitor cell formation through transcriptional control of Snail and E-
797 cadherin. Nat Genet *42*, 89-93. 10.1038/ng.494.
798 65. Essafi, A., Webb, A., Berry, R.L., Slight, J., Burn, S.F., Spraggon, L., Velecela, V.,
799 Martinez-Estrada, O.M., Wiltshire, J.H., Roberts, S.G., et al. (2011). A wt1-controlled
800 chromatin switching mechanism underpins tissue-specific wnt4 activation and
801 repression. Dev Cell *21*, 559-574. 10.1016/j.devcel.2011.07.014.
802 66. Tontonoz, P., Hu, E., and Spiegelman, B.M. (1994). Stimulation of adipogenesis in
803 fibroblasts by PPAR gamma 2, a lipid-activated transcription factor. Cell *79*, 1147-1156.
804 10.1016/0092-8674(94)90006-x.
805 67. Michelson, D.A., Hase, K., Kaisho, T., Benoist, C., and Mathis, D. (2022). Thymic
806 epithelial cells co-opt lineage-defining transcription factors to eliminate autoreactive T
807 cells. Cell *185*, 2542-2558 e2518. 10.1016/j.cell.2022.05.018.
808 68. Mandel-Brehm, C., Vazquez, S.E., Liverman, C., Cheng, M., Quandt, Z., Kung, A.F.,
809 Parent, A., Miao, B., Disse, E., Cugnet-Anceau, C., et al. (2023). Autoantibodies to
810 Perilipin-1 Define a Subset of Acquired Generalized Lipodystrophy. Diabetes *72*, 59-70.
811 10.2337/db21-1172.
812 69. Agarwal, S., Bodansky, A., Xing, C., Anderson, M.S., and Garg, A. (2024). Partial
813 Lipodystrophy Affecting the Extremities in a Young Woman With Autoimmune
814 Polyglandular Syndrome 1. JCEM Case Rep *2*, luae166. 10.1210/jcemcr/luae166.
815 70. Youm, Y.H., Yang, H., Sun, Y., Smith, R.G., Manley, N.R., Vandanmagsar, B., and Dixit,
816 V.D. (2009). Deficient ghrelin receptor-mediated signaling compromises thymic stromal
817 cell microenvironment by accelerating thymic adiposity. J Biol Chem *284*, 7068-7077.
818 10.1074/jbc.M808302200.

71. Yang, H., Youm, Y.H., Sun, Y., Rim, J.S., Galban, C.J., Vandanmagsar, B., and Dixit, V.D. (2009). Axin expression in thymic stromal cells contributes to an age-related increase in thymic adiposity and is associated with reduced thymopoiesis independently of ghrelin signaling. J Leukoc Biol *85*, 928-938. 10.1189/jlb.1008621.
72. Yang, H., Youm, Y.H., Vandanmagsar, B., Rood, J., Kumar, K.G., Butler, A.A., and Dixit, V.D. (2009). Obesity accelerates thymic aging. Blood *114*, 3803-3812. 10.1182/blood-2009-03-213595.
73. Sheridan, J.M., Keown, A., Policheni, A., Roesley, S.N.A., Rivlin, N., Kadouri, N., Ritchie, M.E., Jain, R., Abramson, J., Heng, T.S.P., and Gray, D.H.D. (2017). Thymospheres Are Formed by Mesenchymal Cells with the Potential to Generate Adipocytes, but Not Epithelial Cells. Cell Rep *21*, 934-942. 10.1016/j.celrep.2017.09.090.
74. Venables, T., Griffith, A.V., DeAraujo, A., and Petrie, H.T. (2019). Dynamic changes in epithelial cell morphology control thymic organ size during atrophy and regeneration. Nat Commun *10*, 4402. 10.1038/s41467-019-11879-2.
75. Givony, T., Leshkowitz, D., Del Castillo, D., Nevo, S., Kadouri, N., Dassa, B., Gruper, Y., Khalaila, R., Ben-Nun, O., Gome, T., et al. (2023). Thymic mimetic cells function beyond self-tolerance. Nature *622*, 164-172. 10.1038/s41586-023-06512-8.
76. Zhu, X., Gui, J., Dohkan, J., Cheng, L., Barnes, P.F., and Su, D.M. (2007). Lymphohematopoietic progenitors do not have a synchronized defect with age-related thymic involution. Aging Cell *6*, 663-672. 10.1111/j.1474-9726.2007.00325.x.
77. Oh, J., Wang, W., Thomas, R., and Su, D.M. (2020). Thymic rejuvenation via FOXN1-reprogrammed embryonic fibroblasts (FREFs) to counteract age-related inflammation. JCI Insight *5*. 10.1172/jci.insight.140313.
78. Kim, M.J., Miller, C.M., Shadrach, J.L., Wagers, A.J., and Serwold, T. (2015). Young, proliferative thymic epithelial cells engraft and function in aging thymuses. J Immunol *194*, 4784-4795. 10.4049/jimmunol.1403158.
79. Bredenkamp, N., Nowell, C.S., and Blackburn, C.C. (2014). Regeneration of the aged thymus by a single transcription factor. Development *141*, 1627-1637. 10.1242/dev.103614.
80. Stuart, T., Butler, A., Hoffman, P., Hafemeister, C., Papalexi, E., Mauck, W.M., 3rd, Hao, Y., Stoeckius, M., Smibert, P., and Satija, R. (2019). Comprehensive Integration of Single-Cell Data. Cell *177*, 1888-1902 e1821. 10.1016/j.cell.2019.05.031.
81. Stuart, T., Srivastava, A., Madad, S., Lareau, C.A., and Satija, R. (2021). Single-cell chromatin state analysis with Signac. Nat Methods *18*, 1333-1341. 10.1038/s41592-021-01282-5.
82. Sergushichev, A.A. (2016). An algorithm for fast preranked gene set enrichment analysis using cumulative statistic calculation. bioRxiv *060012*. https://doi.org/10.1101/060012.

Figure 1

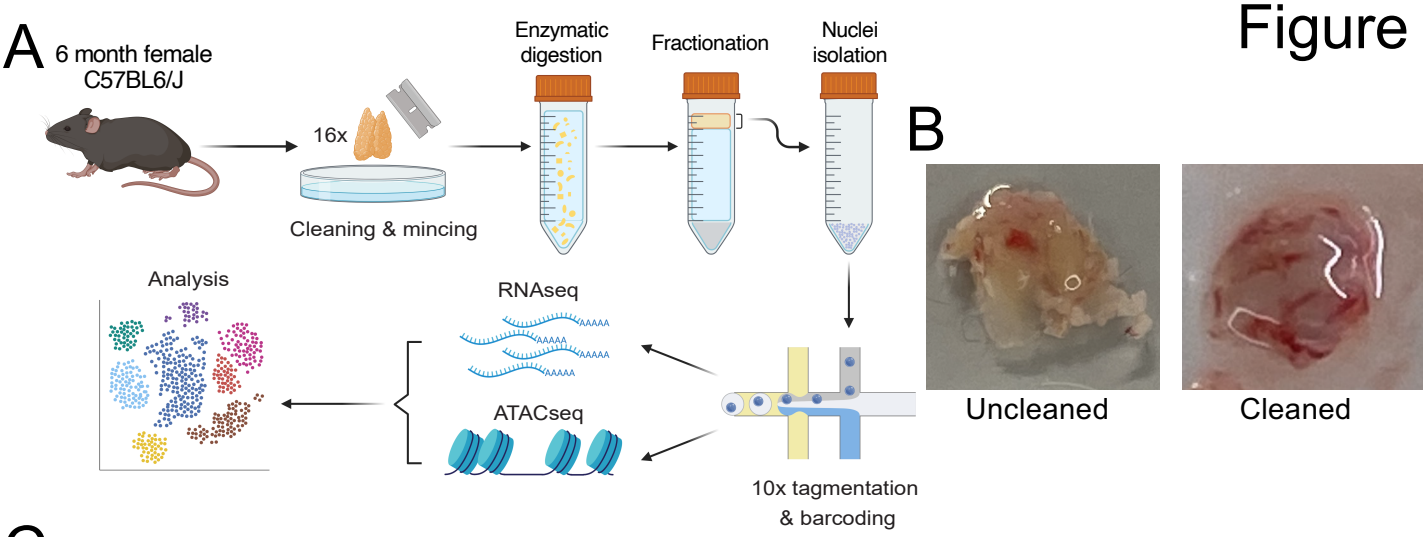
A
6 month female
C57BL6/J
16x
Cleaning & mincing
Enzymatic digestion
Fractionation
Nuclei isolation
Analysis
RNAseq
ATACseq
10x tagmentation & barcoding
B
Uncleaned
Cleaned

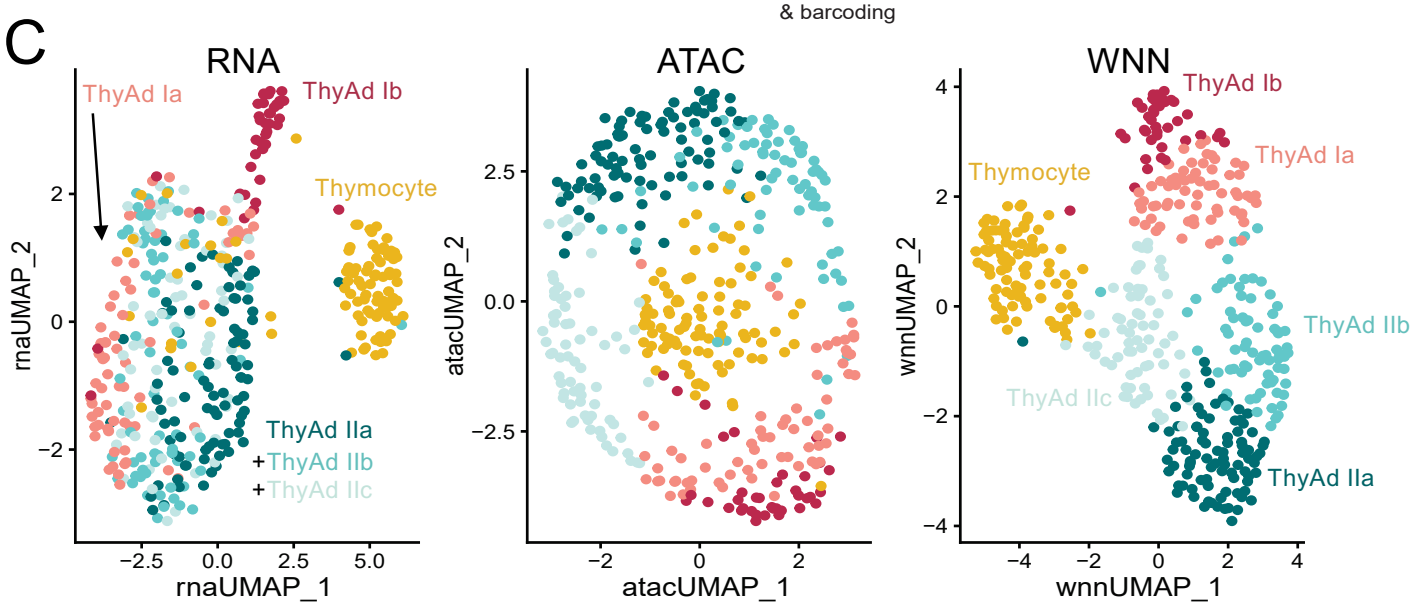
C
RNA
ATAC
WNN
ThyAd Ia
ThyAd Ib
Thymocyte
ThyAd IIa
+ThyAd IIb
+ThyAd IIc
ThyAd IIb
ThyAd IIc
rnaUMAP_1
rnaUMAP_2
atacUMAP_1
atacUMAP_2
wnnUMAP_1
wnnUMAP_2

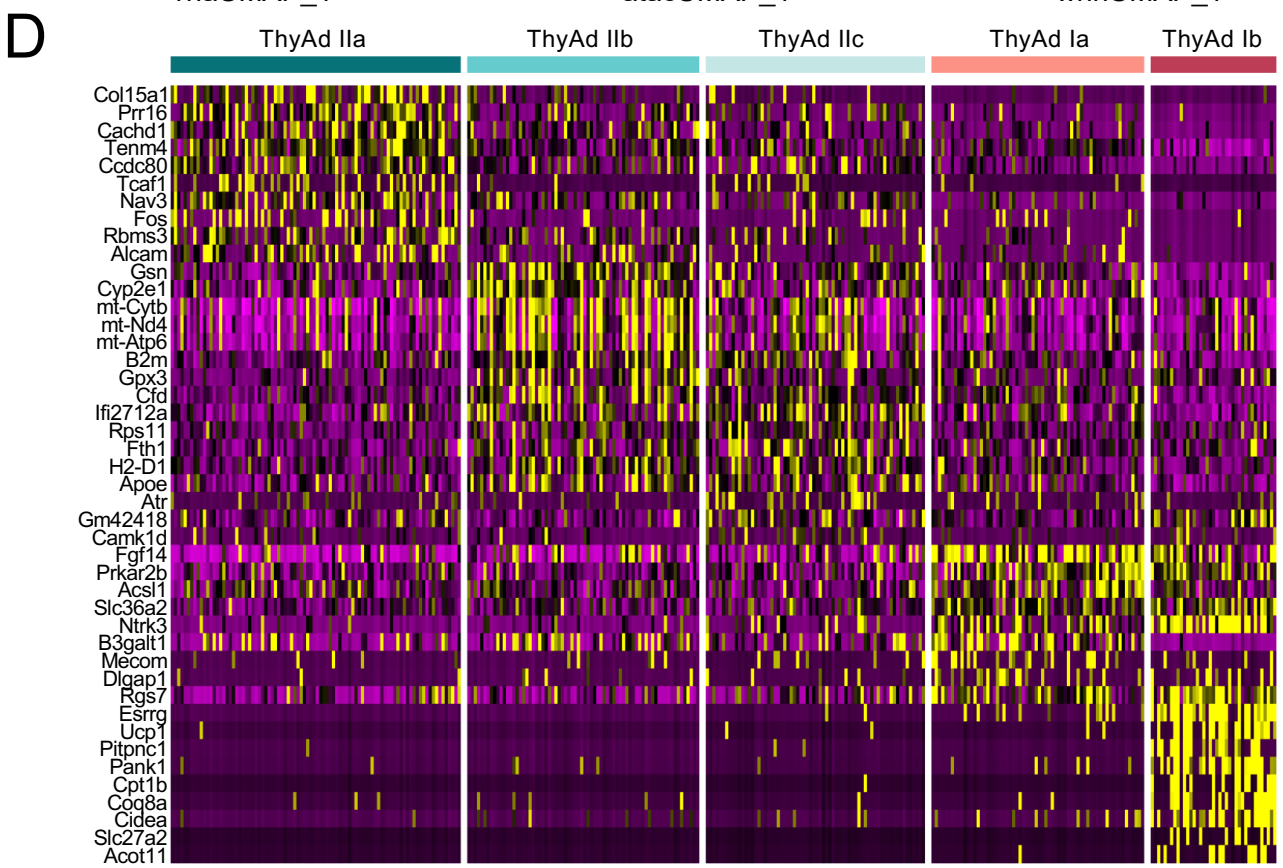
D
ThyAd IIa
ThyAd IIb
ThyAd IIc
ThyAd Ia
ThyAd Ib
Col15a1
Prr16
Cachd1
Tenm4
Ccdc80
Tcaf1
Nav3
Fos
Rbms3
Alcam
Gsn
Cyp2e1
mt-Cytb
mt-Nd4
mt-Atp6
B2m
Gpx3
Cfd
Ifi2712a
Rps11
Fth1
H2-D1
Apoe
Atr
Gm42418
Camk1d
Fgf14
Prkar2b
Acsl1
Slc36a2
Ntrk3
B3galt1
Mecom
Dlgap1
Rgs7
Esrrg
Ucp1
Pitpnc1
Pank1
Cpt1b
Coq8a
Cidea
Slc27a2
Acot11

Figure 2

A

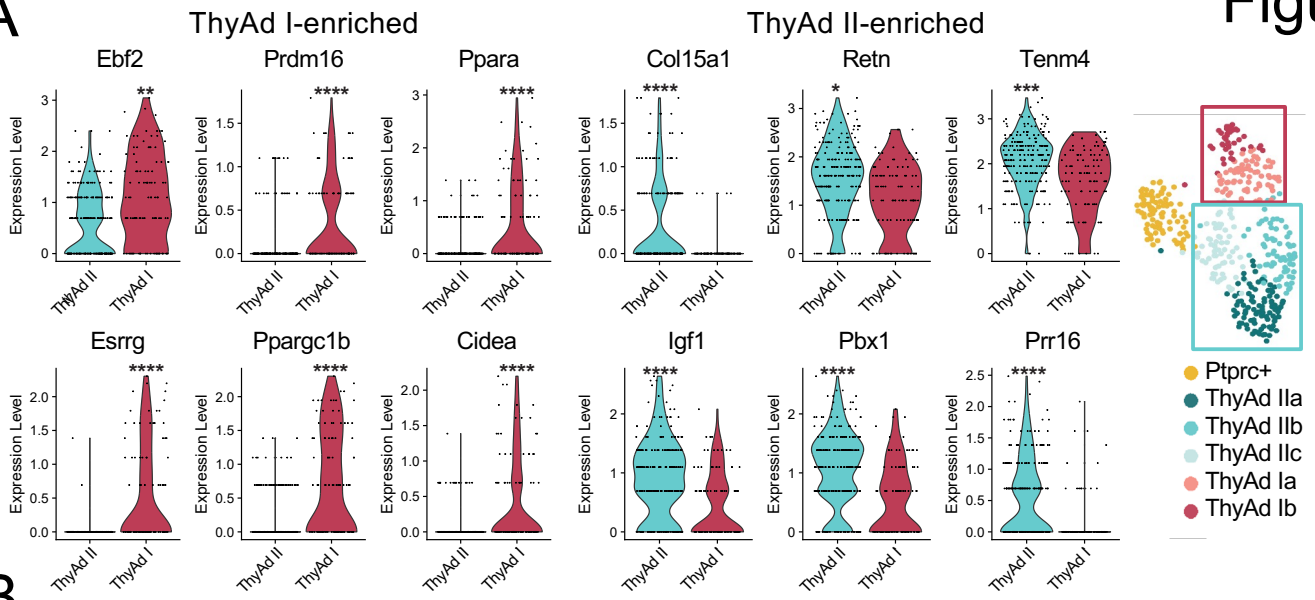

B

ThyAd I GO-Biological Process	NES	pval
Apoptotic mitochondrial changes	2.87	5.5E-04
Regulation of membrane potential	2.69	5.7E-04
Mitochondrial organization	2.39	7.8E-04
Regulation of anatomical structure morphogenesis	2.37	6.4E-04
Positive regulation of cold induced thermogenesis	2.30	4.9E-03
Sensory organ development	2.28	4.7E-03
Defense response to other organism	2.26	3.2E-03
Learning	2.26	9.5E-03
Regulation of lipid metabolic process	2.15	5.8E-03
Electron transport chain	2.12	9.6E-03
Regulation of cell projection organization	2.08	4.6E-03
ThyAd I GO-Hallmark	**NES**	**pval**
Estrogen response early	2.40	5.6E-03
Adipogenesis	2.24	4.3E-03

ThyAd II GO-Biological Process	NES	pval
Cell adhesion	2.68	1.9E-05
Extrinsic apoptotic signaling pathway	2.63	1.5E-03
Regulation of endothelial cell migration	2.61	5.0E-04
Negative regulation of developmental process	2.45	3.1E-04
Response to inorganic substance	2.30	2.2E-03
ATP synthesis coupled electron transport	2.30	5.4E-03
Regulation of locomotion	2.27	5.1E-04
Positive regulation of cellular catabolic process	2.16	9.9E-03
Regulation of cell population proliferation	2.02	3.4E-03
ThyAd II GO-Hallmark	**NES**	**pval**
Bile acid metabolism	2.26	6.6E-03
Epithelial mesenchymal transition	2.25	7.2E-03

Figure 3

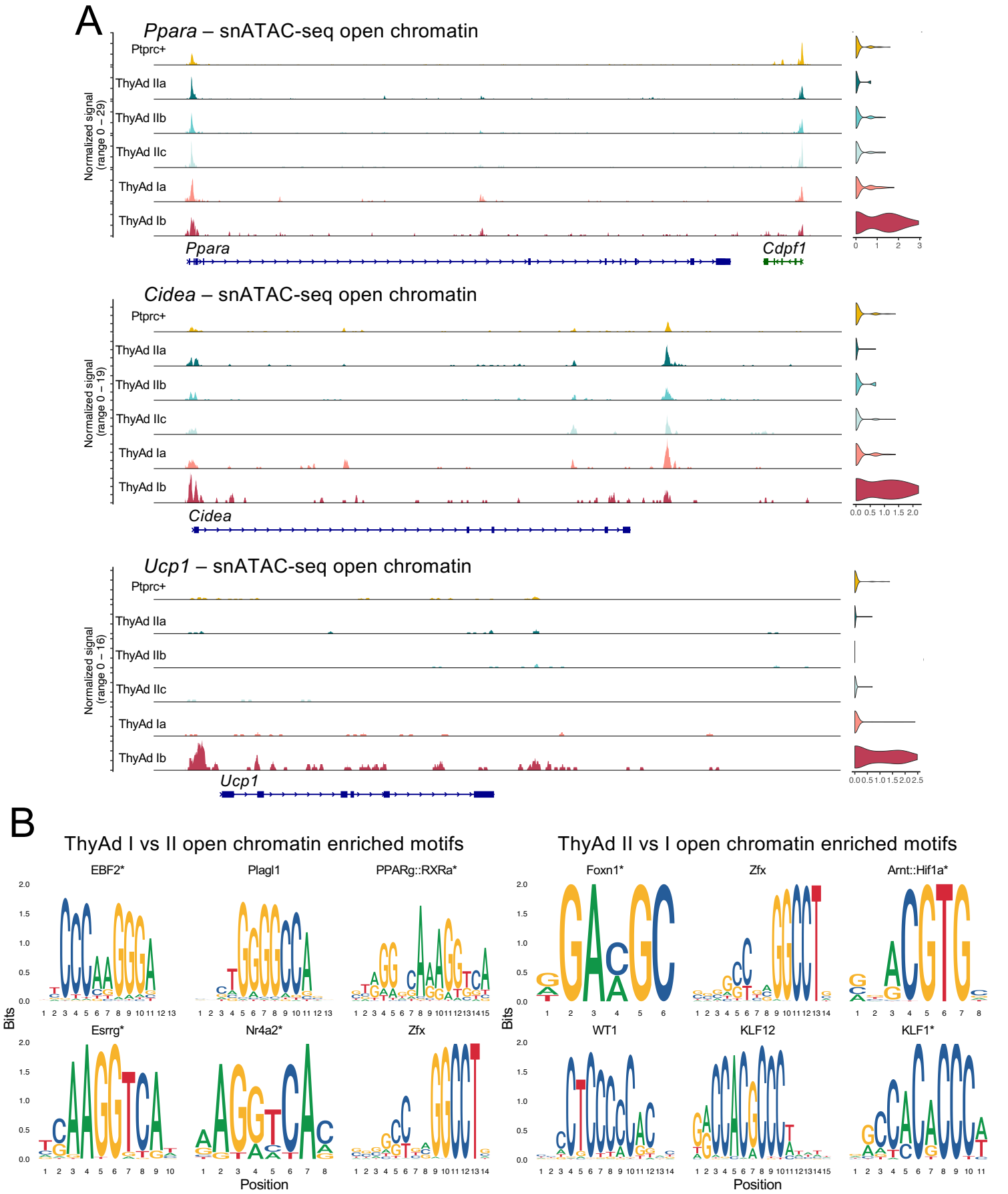
A
Ppara – snATAC-seq open chromatin
Ptprc+
ThyAd IIa
ThyAd IIb
ThyAd IIc
ThyAd Ia
ThyAd Ib
Normalized signal (range 0 – 29)
Ppara
Cdpf1
Cidea – snATAC-seq open chromatin
Normalized signal (range 0 – 19)
Cidea
Ucp1 – snATAC-seq open chromatin
Normalized signal (range 0 – 16)
Ucp1
B
ThyAd I vs II open chromatin enriched motifs
EBF2*
Plagl1
PPARg::RXRa*
Esrrg*
Nr4a2*
Zfx
ThyAd II vs I open chromatin enriched motifs
Foxn1*
Zfx
Arnt::Hif1a*
WT1
KLF12
KLF1*
Bits
Position

Figure 4

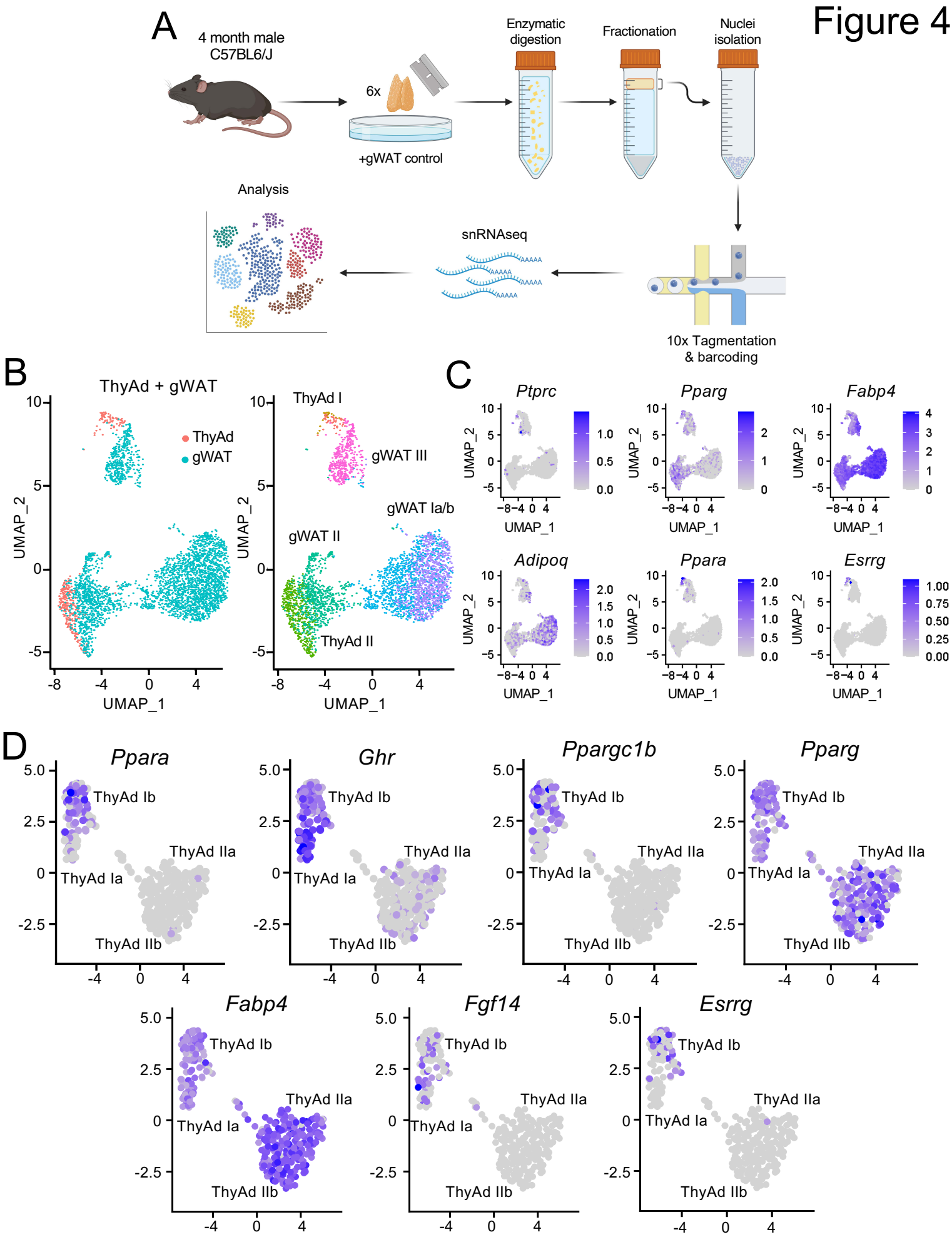
A
4 month male
C57BL6/J
6x
+gWAT control
Enzymatic
digestion
Fractionation
Nuclei
isolation
10x Tagmentation
& barcoding
snRNAseq
Analysis
B
ThyAd + gWAT
ThyAd
gWAT
ThyAd I
gWAT III
gWAT Ia/b
gWAT II
ThyAd II
UMAP_1
UMAP_2
C
Ptprc
Pparg
Fabp4
Adipoq
Ppara
Esrrg
D
Ppara
Ghr
Ppargc1b
Pparg
Fabp4
Fgf14
Esrrg
ThyAd Ib
ThyAd Ia
ThyAd IIa
ThyAd IIb

Figure 5

A

Minus 1° antibody

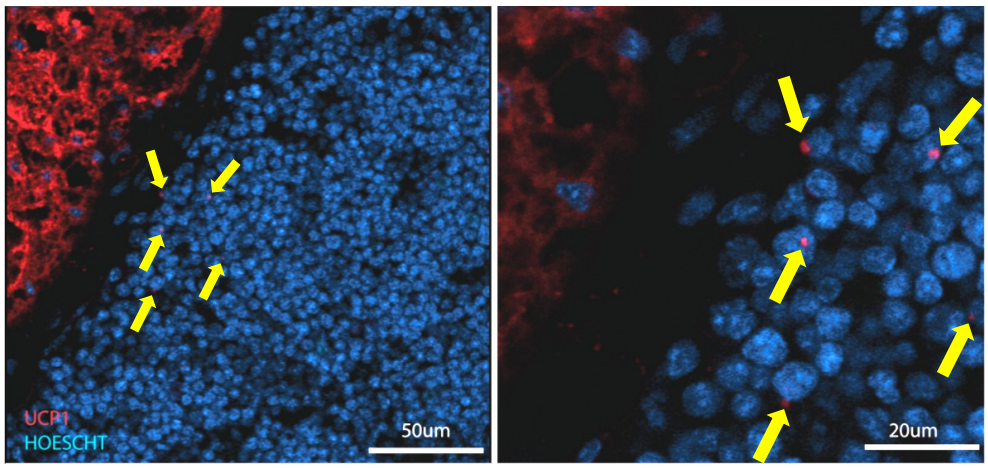

Adjacent section With 1° antibody

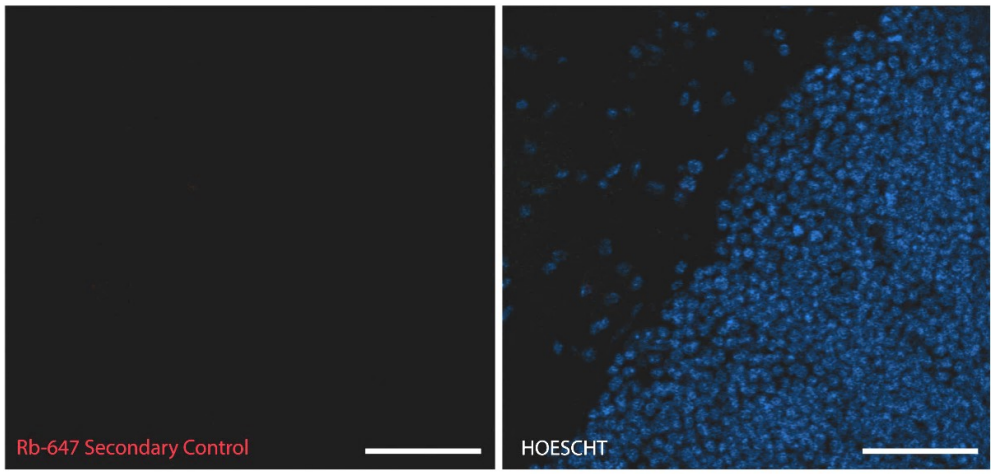

B

Minus 1° antibody

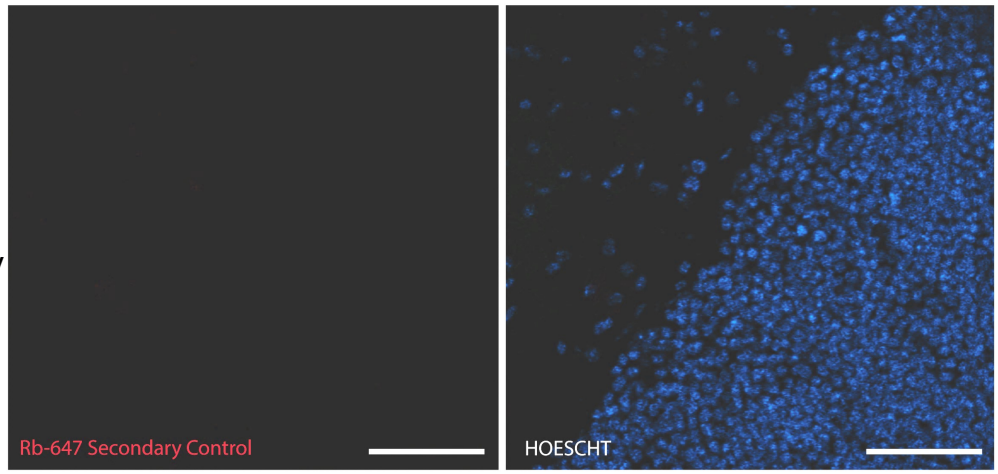
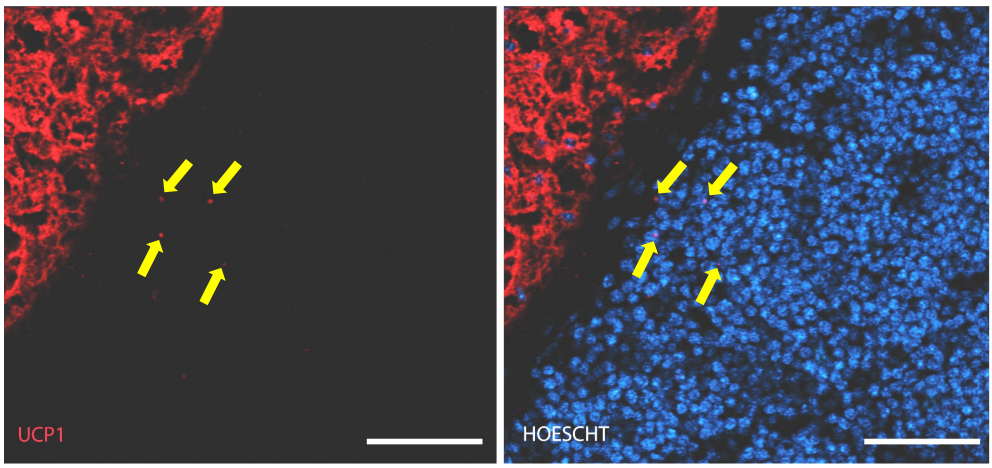
Adjacent section With 1° antibody